


Unusual electromagnetic modes in space-time-modulated dispersion-engineered media

Nima Chamanara, Zoé-Lise Deck-Léger, and Christophe Caloz
Polytechnique Montréal, Montréal, Québec, Canada, H3T 1J4

Dikshitulu Kalluri
University of Massachusetts, Lowell, Massachusetts 01854, USA

 (Received 19 October 2017; revised manuscript received 13 April 2018; published 14 June 2018)

We report on electromagnetic modes in space-time-modulated dispersion-engineered media. These modes exhibit unusual dispersion relation, field profile, and scattering properties. They are generated by coupled codirectional space-time harmonic pairs and occur in space-time periodic media whose constituent materials exhibit specific dispersion. Excitation of a slab of such a medium with *subluminal* modulation results in periodic transfer of energy between the incident frequency and a frequency shifted by a multiple of the modulation frequency, whereas *superluminal* modulation generates exponentially growing anharmonics. These modes may find applications in optical mixers, terahertz sources, and other optical devices.

DOI: [10.1103/PhysRevA.97.063829](https://doi.org/10.1103/PhysRevA.97.063829)

I. INTRODUCTION

Periodic structures are an essential part of modern photonic and microwave technologies. Electromagnetic band gaps emerging from such structures play a crucial role in many applications, including photonic crystal waveguides [1], filters [2], fiber gratings [3], etc. These band gaps support evanescent electromagnetic modes characterized by complex propagation numbers, i.e., exponential decay in space [1].

The temporal counterparts [4] of conventional photonic crystals, termed *temporal photonic crystals*, have been shown to exhibit complex frequencies or vertical band gaps, as opposed to horizontal band gaps in spatial photonic crystals [5,6]. They represent electromagnetic media whose constitutive parameters vary periodically in time [5–7]. Their vertical band gaps describe instabilities [8], where the amplitude of electromagnetic waves grows and/or decays exponentially, i.e., with $e^{\pm\omega t}$ time dependence, everywhere in space.

Combining *both* time and space modulations allows one to control not only the orientation—horizontal or vertical—of the band gaps but also their oblique alignment [9–11]. *Subluminal* space-time-modulated structures, where the phase velocity of the modulation (v_m) is smaller than the velocity of light in the background medium (v_b), support obliquely aligned horizontally oriented band gaps, whereas *superluminal* space-time-modulated structures with $v_m > v_b$ support obliquely aligned vertically oriented band gaps [11].

This paper considers periodic space-time-modulated media composed of *dispersive* materials. It shows that the addition of dispersion to space-time modulation brings about a unique diversity of electromagnetic modes. Particularly, such a medium can support new modes with dispersion, field, and scattering properties that are radically different from those accessible in conventional or space-time periodic media composed of *nondispersive* materials.

II. CODIRECTIONAL-COUPLED SPACE-TIME HARMONICS

Consider first the case of space-time periodic media composed of nondispersive materials. The corresponding permittivity for spatiotemporal modulation along z may be written as

$$\epsilon(\mathbf{r}, t) = \epsilon_0 \epsilon_r [1 + M f_{\text{per}}(\omega_m t - \beta_m z)], \quad (1)$$

where $\mathbf{r} = (x, y, z)$, ϵ_r is the permittivity of the nondispersive background medium, M is the modulation depth representing the strength of the modulation, $f_{\text{per}}(\cdot)$ is a periodic real function with period 2π , and ω_m and β_m are temporal and spatial modulation frequencies, respectively. The dispersion relation of the nondispersive background medium (ϵ_r) is plotted in green in Fig. 1(a). Electromagnetic waves in the modulated medium can be expressed in the Floquet-Bloch form [9–11]

$$\mathbf{E}(\mathbf{r}, t) = e^{j(\omega t - \beta z)} \sum_{n=-\infty}^{\infty} \mathbf{E}_n e^{jn(\omega_m t - \beta_m z)}, \quad (2)$$

where β is the Floquet-Bloch wave number. It can be shown from the Fourier expansion in (2) that dispersion curves are periodic along the vector $\mathbf{p}_m = \beta_m \hat{\beta} + \omega_m \hat{\omega}$ [9]. Typical dispersion curves for a vanishingly small modulation depth ($M \rightarrow 0$), called the “empty lattice approximation” in solid-state physics, are plotted in Fig. 1(a). Since the green lines are solutions to dispersion relations in this limit, the rest of the dispersion diagram is obtained by periodically shifting the background dispersion line along \mathbf{p}_m . This provides a very close approximation of the dispersion curves everywhere except at the points where these shifted curves, or space-time harmonics, intersect. The two space-time harmonics forming such intersections are phase matched and hence strongly couple to one another. For a nondispersive background medium, such couplings involve a forward harmonic and a backward harmonic, as emphasized by the circle in Fig. 1(a). In the case of subluminal modulation, as in Fig. 1(a), the resulting forward-

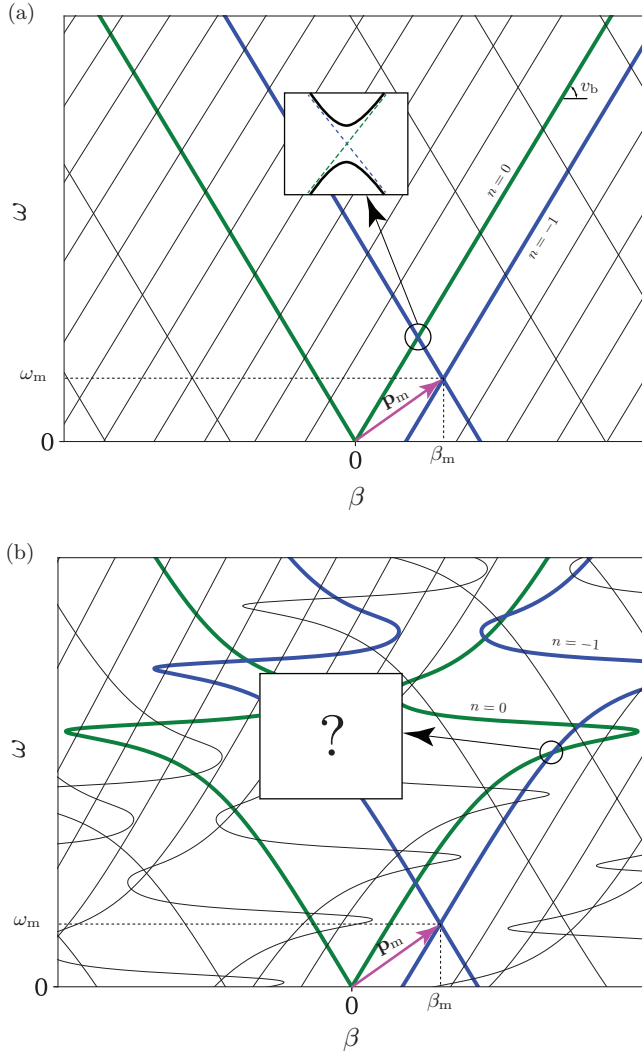


FIG. 1. Comparison of dispersion diagrams of space-time-modulated periodic media composed of nondispersive and dispersive background materials for $M \rightarrow 0$. (a) Case of nondispersive background material. (b) Case of strongly dispersive background material. The magenta arrow shows the modulation (or space-time period) vector (\mathbf{p}_m). Here, unessentially, the modulation for both cases is subluminal ($v_m = \omega_m/\beta_m < v_b$). For clarity, the two space-time harmonics $n = 0$ and $n = -1$ are emphasized.

backward coupling generates evanescent modes, with complex β corresponding to horizontally oriented gaps, as shown in the inset. For a superluminal modulation, the forward-backward coupling between space-time harmonics generates unstable modes, with complex ω corresponding to vertically oriented gaps (inset of Fig. 1(a) rotated by 90°) [9,11].

In such a space-time-modulated periodic medium, composed of *nondispersive* materials, only forward-backward coupling between space-time harmonics is possible, as illustrated in the inset of Fig. 1(a). In contrast, if the background medium is dispersion-engineered [12–16], as in Fig. 1(b), then it is possible to produce codirectional, forward-forward (emphasized by the circle) or backward-backward, coupling harmonic pairs. It is shown in Sec. III how such periodic dispersive space-time harmonics can be generated in a

space-time-modulated dispersive medium. We investigate next such scenarios in a space-time periodic dispersion-engineered medium with Lorentz background material dispersion [17] and the resulting unusual electromagnetic modes emerging from such codirectional couplings for both subluminal and superluminal modulations.

III. CODIRECTIONAL-COUPLED SPACE-TIME HARMONICS IN UNBOUNDED LORENTZ MEDIA

The background material in the dispersive-background medium is described by the following relative Lorentz permittivity:

$$\epsilon_r(\omega) = 1 + \frac{\omega_p^2}{\omega_r^2 + j\gamma\omega - \omega^2}, \quad (3)$$

where ω_r is the Lorentz resonance frequency, $\omega_p = e\sqrt{\frac{n_a}{\epsilon_0 m_e}}$ is the plasma frequency, γ is the relaxation rate, and n_a is the molecular (atomic) density of the material. Such dispersion occurs naturally in dielectric materials [17]. It can also be produced artificially in metamaterials [12,18]. We assume that the material density is spatiotemporally modulated as

$$n_a(\mathbf{r}, t) = n_0[1 + M f_{\text{per}}(\omega_m t - \beta_m z)], \quad (4)$$

which may be practically achieved by a modulated laser in nonlinear materials [19], electric modulation in electro-optic materials [20], acoustic waves in acousto-optic materials [21], and transistors or varactors in electronically controlled metamaterials [10,11].

To find the electromagnetic modes in this medium, equations

$$\nabla \times \nabla \times \mathbf{E}(\mathbf{r}, t) + \mu_0 \frac{\partial^2}{\partial t^2} \mathbf{D}(\mathbf{r}, t) = 0, \quad (5)$$

$$\mathbf{D}(\mathbf{r}, t) = \epsilon_0 \mathbf{E}(\mathbf{r}, t) + \mathbf{P}(\mathbf{r}, t), \quad (6)$$

$$\frac{\partial^2}{\partial t^2} \mathbf{P}(\mathbf{r}, t) + \gamma \frac{\partial}{\partial t} \mathbf{P}(\mathbf{r}, t) + \omega_r^2 \mathbf{P}(\mathbf{r}, t) = \frac{n_a(\mathbf{r}, t) e^2}{m_e} \mathbf{E}(\mathbf{r}, t), \quad (7)$$

which are the wave equation, the displacement field equation, and the classical Newton equation for a Lorentz medium [17], respectively, are solved self-consistently. The solution of the problem is found by expressing all the field quantities in these equations in terms of the space-time Floquet-Bloch expansion

$$\Psi(\mathbf{r}, t) = e^{j(\omega t - \beta z)} \sum_{n=-\infty}^{\infty} \Psi_n e^{jn(\omega_m t - \beta_m z)}, \quad (8)$$

where $\Psi = \mathbf{E}, \mathbf{P}, \mathbf{D}$, and $\Psi_n = \mathbf{E}_n, \mathbf{P}_n, \mathbf{D}_n$ are complex constants. A straightforward Fourier analysis then provides the dispersion curves and the electromagnetic fields. (See Appendix A for details.)

A. Subluminal modulation

Consider, as an example, a lossless Lorentz medium with normalized parameters $\omega_p/\omega_r = 0.6$ and $\gamma/\omega_r \rightarrow 0$ (lossless). The background material density is modulated as in (4), with spatial and temporal modulation frequencies $\beta_m =$

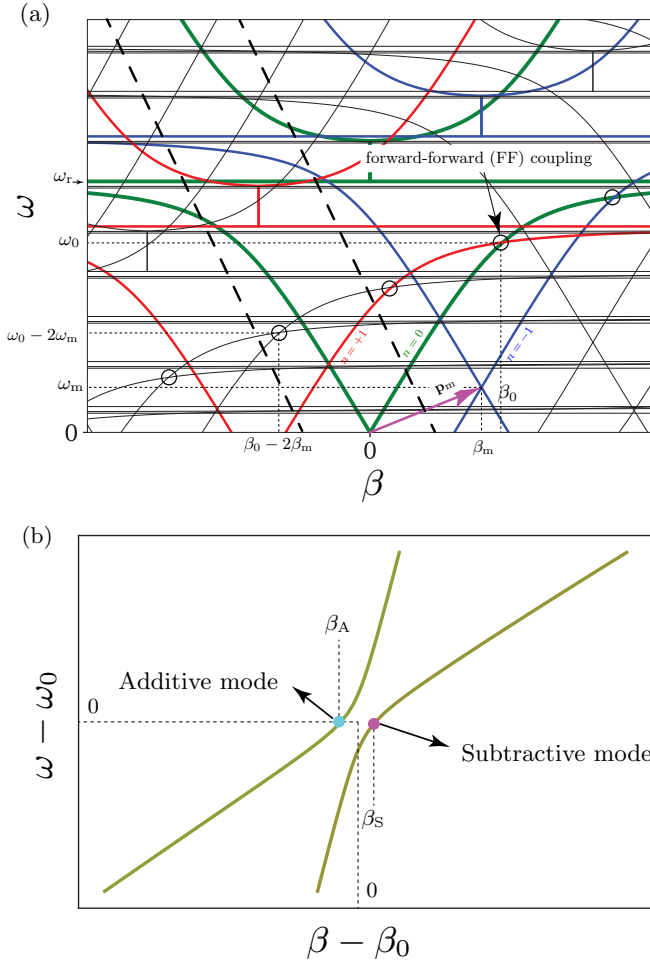


FIG. 2. (a) Dispersion diagram of a subluminaly space-time-modulated lossless Lorentz medium for $M \rightarrow 0$. The magenta arrow represents the modulation vector. The three space-time harmonics $n = 0$ (green), $n = +1$ (red), and $n = -1$ (blue) are emphasized. The dashed lines represent the edges of the Brillouin zone. (b) Dispersion diagram zoomed in at the crossing circled in Fig. 2(a) for the finite modulation depth $M = 0.01$ and $f_{\text{per}}(\cdot) = \cos(\cdot)$. The solid curves represent the real parts of the dispersion. The imaginary parts are zero.

$0.8673\omega_r/c$ and $\omega_m = 0.18\omega_r$, respectively. The corresponding dispersion curves are plotted in Fig. 2(a) for $M \rightarrow 0$. Note that the dispersion curves are periodic along the *oblique* modulation vector \mathbf{p}_m and therefore the Brillouin zone, representing the smallest period containing all the dispersion information, is also oblique, as represented by the dashed lines in Fig. 2(a). Points on the dispersion curves connected by integer multiples of the periodicity vector \mathbf{p}_m are equivalent and may be represented by the same point in the Brillouin zone.

Consider the intersections between forward space-time harmonics emphasized by the circles in Fig. 2(a). Note that these points are connected by integer multiples of the modulation vector \mathbf{p}_m and therefore all represent the same mode. Next we calculate the dispersion curves and the corresponding

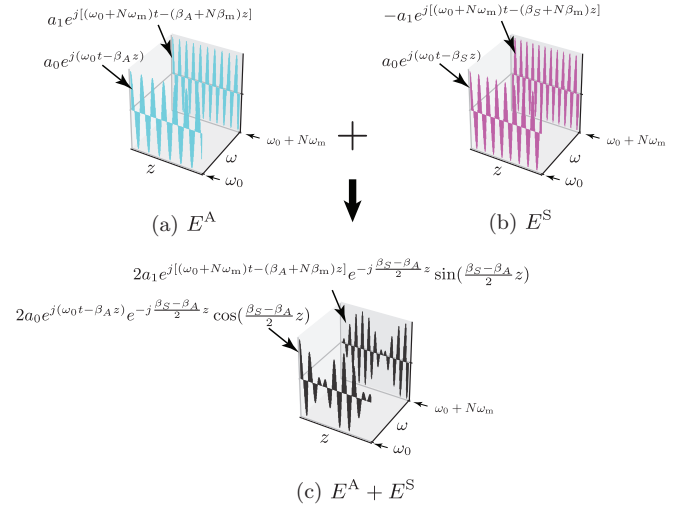


FIG. 3. Field profiles for (a) the additive mode (E^A), corresponding to the cyan point in Fig. 2(b), and (b) the subtractive mode (E^S), corresponding to the purple point in Fig. 2(b), and (c) their superposition ($E^A + E^S$).

electromagnetic fields emerging from such forward-forward coupling for finite modulation depths.

In the case of a finite nonzero modulation depth, these space-time harmonics couple to each other as a result of phase matching. Consider the forward-forward intersection at the point (ω_0, β_0) in Fig. 2(a). The two crossing space-time harmonics are $n = 0$, i.e., $e^{j(\omega t - \beta z)}$ and $n = +1$, i.e., $e^{j[(\omega + \omega_m)t - (\beta + \beta_m)z]}$. At the crossing point (ω_0, β_0) these harmonics are given by $e^{j(\omega_0 t - \beta_0 z)}$ and $e^{j[(\omega_0 + \omega_m)t - (\beta_0 + \beta_m)z]}$, respectively. Note that we would have made the same conclusion considering any other equivalent circled intersection in Fig. 2(a). As an example, consider the circled intersection inside the Brillouin zone located at the point $(\omega_0 - 2\omega_m, \beta_0 - 2\beta_m)$. The intersecting harmonics at this point are $n = +2$, i.e., $e^{j[(\omega + 2\omega_m)t - (\beta + 2\beta_m)z]}$, and $n = +3$, i.e., $e^{j[(\omega + 3\omega_m)t - (\beta + 3\beta_m)z]}$. At their crossing point $(\omega_0 - 2\omega_m, \beta_0 - 2\beta_m)$, these harmonics are given as before by $e^{j(\omega_0 t - \beta_0 z)}$ and $e^{j[(\omega_0 + \omega_m)t - (\beta_0 + \beta_m)z]}$, respectively, which is expected by the periodicity of the dispersion curves.

As a result of coupling between these two harmonics for finite nonzero modulation depths, the dispersion curves at the intersection point changes and new electromagnetic modes emerge. The resulting dispersion curves, zoomed in at the intersection points, calculated numerically using Fourier-Bloch analysis described in Appendix A, are plotted in Fig. 2(b). Note that the frequency and the propagation constant are purely real. At a fixed frequency ω_0 , two modes with slightly different propagation constants have emerged. For a relatively small modulation depth $M \ll 1$, the electromagnetic fields of these modes are computed in Appendix B as

$$E_A = a_0 e^{j(\omega_0 t - \beta_A z)} + a_1 e^{j[(\omega_0 + N\omega_m)t - (\beta_A + N\beta_m)z]}, \quad (9a)$$

$$E_S = a_0 e^{j(\omega_0 t - \beta_S z)} - a_1 e^{j[(\omega_0 + N\omega_m)t - (\beta_S + N\beta_m)z]}, \quad (9b)$$

where the subscripts A and S stand for “additive” and “subtractive,” respectively, in reference with the signs in (9), and are plotted in Figs. 3(a) and 3(b) for $M = 0.01$. Here N is an

integer equal to the difference between the harmonic index of the crossing space-time harmonics ($N = 1$ in Fig. 2(a)).

In contrast to forward-backward crossings in subluminal nondispersive systems, such as in static photonic crystals, which produce complex modes, the modes in Fig. 2(b) have *purely real*, but slightly distinct wave numbers and contain the frequencies of the coupled space-time harmonics at the crossing point, i.e., $e^{j\omega_0 t}$ and $e^{j(\omega_0 + N\omega_m)t}$ [Eq. (9)]. Figures 3(a) and 3(b) show the field plots for the additive and subtractive modes, respectively, where the harmonics at ω_0 and $\omega_1 = \omega_0 + N\omega_m$ are plotted separately in green and red, respectively. The superposition of these two modes are plotted in Fig. 3(c). Note that, due to the slight difference in the propagation constants of the additive and subtractive modes, the resulting superposed harmonics at ω_0 and $\omega_1 = \omega_0 + N\omega_m$ are periodic and out of phase, with \cos and \sin spatial dependence, respectively. The consequence of such field profiles is explained later when electromagnetic scattering from such media is discussed.

B. Superluminal modulation

Next consider a superluminal modulation for a lossless Lorentz medium with the same background parameters as in the subluminal case ($\omega_p/\omega_r = 0.6$ and $\gamma/\omega_r = 0$). The density of the medium is again modulated as in (4) but with the superluminal spatial-temporal modulation $[\beta_m, \omega_m] = [0.0724\omega_r/c, 0.64\omega_r]$. The corresponding dispersion curves are plotted in Fig. 4(a) for $M \rightarrow 0$, where the crossing (or phase-matched) space-time harmonics are emphasized by circles. As in the subluminal case, these intersections are all equivalent, as they are connected by integer multiples of the modulation vector as vector \mathbf{p}_m .

In the case of a finite modulation depth, these space-time harmonics couple to each other as a result of phase matching. Consider the forward-forward intersection at the point (ω_0, β_0) in Fig. 4(a). The two crossing space-time harmonics are $n = 0$, i.e., $e^{j(\omega t - \beta z)}$ and $n = +1$, i.e., $e^{j[(\omega + \omega_m)t - (\beta + \beta_m)z]}$. At the crossing point (ω_0, β_0) these harmonics are given by $e^{j(\omega_0 t - \beta_0 z)}$ and $e^{j[(\omega_0 + \omega_m)t - (\beta_0 + \beta_m)z]}$, respectively. Note that, similar to the subluminal case, we would have made the same conclusion considering any other equivalent circled intersection in Fig. 4(a).

As a result of coupling between these two harmonics for finite modulation depths, the dispersion curves at the intersection point change and new electromagnetic modes emerge. The resulting dispersion curves, zoomed in at the intersection points, calculated numerically using Fourier-Bloch analysis described in Appendix A, are plotted in Fig. 4(b). Note that superluminal interaction between forward (codirectional) harmonics produces complex propagation constants. At frequencies close to ω_0 , two modes with complex conjugate propagation constants have emerged. For a relatively small modulation depth $M \ll 1$, the electromagnetic fields of the modes emerging from such forward-forward (FF) coupling are computed in Appendix B as

$$E_G = a_0 e^{j(\omega_0 t - \beta_G z)} + a_1 e^{j[(\omega_0 + N\omega_m)t - (\beta_G + N\beta_m)z]}, \quad (10a)$$

$$E_D = a_0 e^{j(\omega_0 t - \beta_D z)} - a_1 e^{j[(\omega_0 + N\omega_m)t - (\beta_D + N\beta_m)z]}, \quad (10b)$$

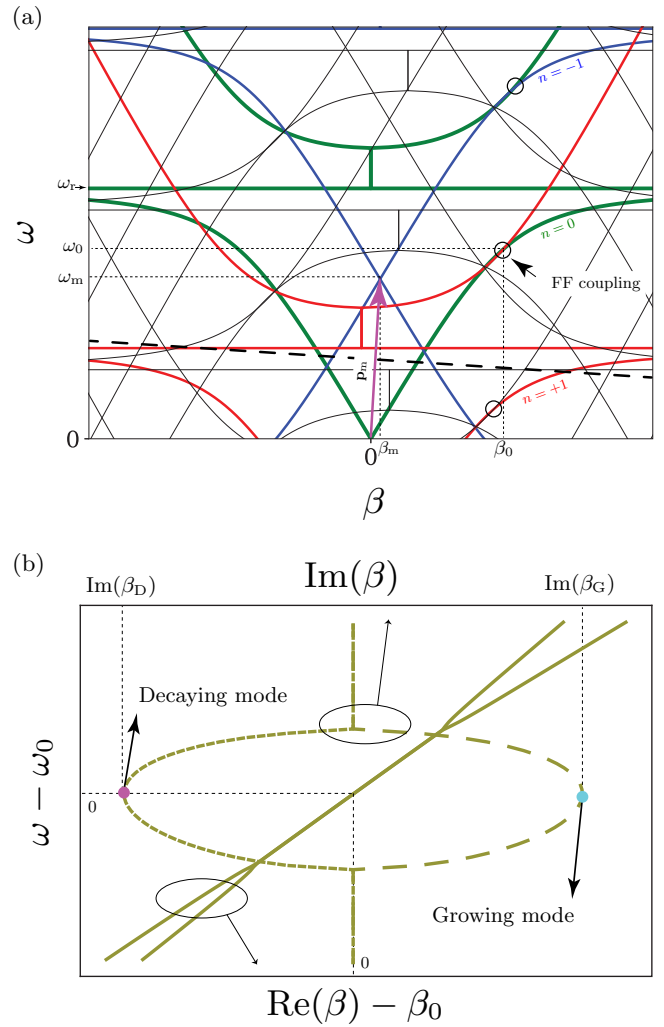


FIG. 4. (a) Dispersion curves of a superluminal space-time modulated Lorentz medium for $M \rightarrow 0$. The magenta arrow represents the modulation vector. The three space-time harmonics $n = 0$ (green), $n = +1$ (red), $n = -1$ (blue) are emphasized. The dashed line represents the edge of the Brillouin zone. (b) Dispersion diagram zoomed in at the crossing circled in Fig. 4(a) for the finite modulation depth $M = 0.01$ and $f_{\text{per}}(\cdot) = \cos(\cdot)$. The solid and dashed curves represent the real and imaginary parts of the propagation constant, respectively.

where the subscripts G and D stand for “growing” and “decaying,” respectively, and are plotted in Figs. 5(a) and 5(b) for $M = 0.01$.

In contrast to forward-backward intersections in nondispersive superluminal periodic media, such as temporal photonic crystals that produce complex frequencies, forward-forward superluminal intersections produce modes with complex conjugate wave numbers, $\beta_G = \beta + j\alpha$ and $\beta_D = \beta - j\alpha$, corresponding to exponentially growing and decaying modes along z , respectively. Note that in contrast to evanescent modes in subluminal space-time periodic media, that are also described by complex conjugate wave numbers; the modes in Fig. 4(b) carry *real nonzero* Poynting power and therefore describe growing and/or decaying *propagating* modes. Evanescent

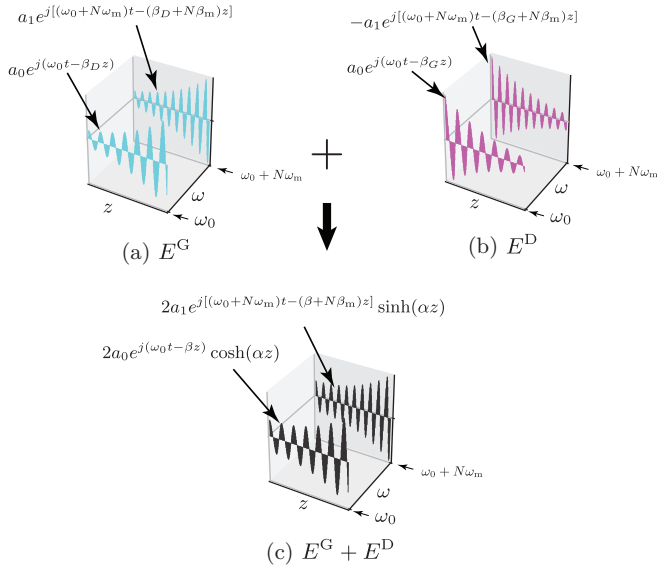


FIG. 5. Field profiles for (a) the growing mode (E^G), corresponding to the cyan point in Fig. 4(b), and (b) the decaying mode (E^D), corresponding to the purple point in Fig. 4(b), and (c) their superposition ($E^G + E^D$), where $\beta = \text{Re}(\beta_G) = \text{Re}(\beta_D)$, $\alpha = \text{Im}(\beta_G) = -\text{Im}(\beta_D)$.

modes, however, carry no real power, i.e., the real part of their Poynting vector is zero along the direction of the waveguide.

As in the subluminal case, the temporal spectrum of the modes in Fig. 4(b) consists of the two frequencies ω_0 and $\omega_0 + N\omega_m$, where N is an integer equal to the difference between the harmonic index of the crossing space-time harmonics ($N = 1$ in Fig. 4(a)). Figures 5(a) and 5(b) show the field plots for the growing and decaying modes, respectively, where the harmonics at ω_0 and $\omega_1 = \omega_0 + N\omega_m$ are plotted separately in green and red, respectively. The superposition of these two modes are plotted in Fig. 5(c). Note that due to the nonzero imaginary part of the propagation constant, the resulting superposed harmonics at ω_0 and $\omega_1 = \omega_0 + N\omega_m$ grow exponentially with \cosh and \sinh spatial dependence, respectively. The consequence of such field profiles is explained later when electromagnetic scattering from such media is discussed.

IV. SCATTERING BY A FINITE SLAB

Next a slab of a space-time periodic Lorentz material is excited by a plane wave, and reflected and transmitted fields as well as the modes excited inside the slab are computed using the full-wave mode-matching technique (see Appendix C for details). This technique provides a great deal of physical insight into the physics of the system, since it provides exact information on the contribution of the unbounded slab contributing to the different waves. Moreover, it is immune to most of the numerical errors that plague other full-wave numerical techniques, such as numerical dispersion error and errors associated with absorbing boundary conditions and excitation models.

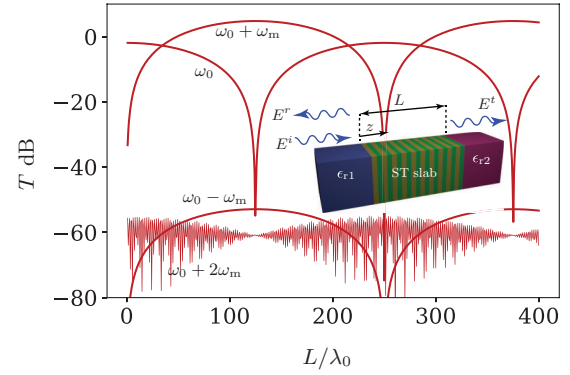


FIG. 6. Transmission power in dB scale, $T = 20 \log_{10} |E^t|/|E^i|$, through a slab of the medium in Fig. 2(b) excited by a plane wave versus its length L . The magnitude of different transmitted harmonics at $\omega_0 + n\omega_m$ are plotted separately.

A. Subluminal modulation

In the subluminal case, the incident wave must be matched to the additive and subtractive modes (9) in order to excite them effectively. Note that at $z = 0$, the superposition of the two modes, $E = \frac{1}{2}(E_A + E_S) = ae^{j\omega_0 t}$, include only the frequency ω_0 and, since $\beta_A \approx \beta_S \approx \beta_0$, an incident plane wave $E^i = \hat{x}e^{j(\omega_0 t - \beta_0 z)}$ is well matched to $E = \frac{1}{2}(E_A + E_S)$ and excites E_A and E_S equally. Therefore, the incident medium should either have the permittivity $\epsilon_{r1} = (\omega_0/c\beta_0)^2$ or be matched to such a permittivity through a matching section in order to excite these modes efficiently.

Figure 6 shows the spectrum of the field transmitted through the slab versus its length for a slab with subluminal space-time-modulated Lorentz medium in Fig. 2(b) excited by a plane wave $E^i = \hat{x}e^{j(\omega_0 t - \beta_0 z)}$. Note that electromagnetic energy is periodically transferred between the harmonics at ω_0 and $\omega_0 + \omega_m$, while the rest of the harmonics are more than 50 dB weaker. At the coherence length, a maximum of energy, possibly with gain due the energy of the modulation, is transferred to the $\omega_0 + \omega_m$ harmonic without any undesirable intermodulation effects, in contrast to what occurs in conventional modulators or mixers. This process is similar to energy exchange between two forward coupled waveguides. Since the additive and subtractive modes in (9) have a slightly different propagation constant, their harmonics at ω_0 acquire some gradual phase mismatch as they propagate along the structure, until they completely fall out of phase at the coherence length, while their harmonics at $\omega_0 + \omega_m$ arrive in phase at the coherence length, and the process is next reversed and repeated periodically. Note that similar transitions may occur between different states of a space-time-modulated photonic crystal, termed *interband photonic transitions* in the photonics literature in analogy to electronics [22,23]. In this sense, the transitions in Fig. 6 may be called *intradband photonic transitions*.

B. Superluminal modulation

As in the subluminal case, in the superluminal space-time-modulated dispersion-engineered medium shown in Fig. 4(b), an incident wave at frequency ω_0 excites both the growing and decaying modes. Figure 7 presents scattering from a slab of

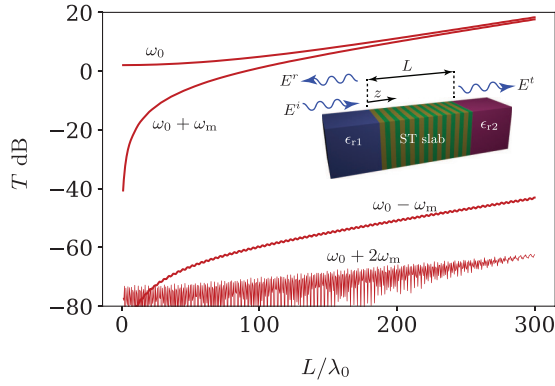


FIG. 7. Transmission power in dB scale, $T = 20 \log_{10} |\mathbf{E}^t|/|\mathbf{E}^i|$, from a slab of the medium in Fig. 4(b) excited by a plane wave, versus its length L . The magnitude of different transmitted harmonics at $\omega_0 + n\omega_m$ are plotted separately.

the superluminal space-time-modulated medium in Fig. 4(b). Note that the transmitted harmonics at ω_0 and $\omega_0 + \omega_m$ grow exponentially as the length of the slab is increased, while the rest of the harmonics are more than 60 dB weaker. The growing mode E_G dominates the exponentially decaying mode E_D as the length of the slab is increased, and since the growing mode contains both harmonics at ω_0 and $\omega_0 + \omega_m$, these harmonics grow exponentially and are transmitted when they reach the other end of the slab.

V. CONCLUSIONS

We study electromagnetic modes in space-time-modulated dispersion-engineered media. It is shown that intercoupling between codirectional space-time harmonics produces electromagnetic modes exhibiting anomalous dispersion relation, field profile, and scattering properties. The most striking results of the paper are summarized in Fig. 8. As a result of *forward-backward* or *contradirectional* space-time harmonic coupling in *subluminal* nondispersive periodic space-time systems shown in Fig. 8(a), evanescent modes characterized by *complex propagation constants* are generated. This paper predicts that *forward-forward* or *codirectional* coupling in *subluminal* dispersive systems, shown in Fig. 8(b), produces purely real propagation constants. As a result of *forward-backward* or *contradirectional* space-time harmonic coupling in *superluminal* nondispersive periodic space-time systems, shown in Fig. 8(c), unstable modes characterized by *complex frequencies* are generated. This paper predicts that *forward-forward* or *codirectional* coupling in *superluminal* dispersive systems, shown in Fig. 8(d), produces *complex propagation constants* describing exponentially growing or decaying propagating modes with real nonzero Poynting power along the direction of propagation.

Excitation of a slab of such dispersive media with *subluminal* modulation results in periodic transfer of energy between the incident frequency and a *single* frequency shifted by a multiple of the modulation frequency, whereas *superluminal* modulation generates *two* exponentially growing anharmonics. These effects may be generated in any strongly dispersive system whose parameters are modulated spatiotemporally, such

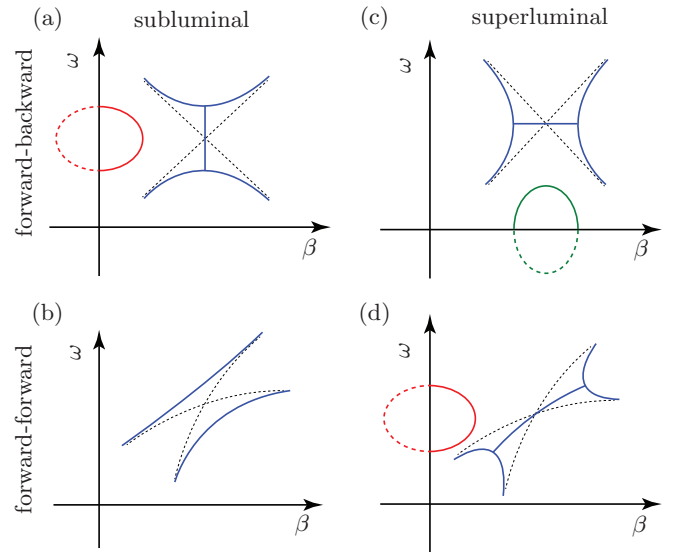


FIG. 8. Different scenarios for intercoupling between space-time harmonics. Top row: nondispersive systems supporting only forward-backward or contradirectional coupling. Bottom row: dispersive systems supporting forward-forward or codirectional space-time harmonic coupling. The left and right columns describe subluminal and superluminal space-time-modulated media, respectively. The dashed black curves represent the background (uncoupled) space-time harmonics. The solid blue curves represent the real parts of the dispersion relations. The red and green curves represent the imaginary parts of the complex propagation constants and complex frequencies, respectively.

that two codirectional space-time harmonics intersect. Such space-time modulation may be produced in nonlinear materials pumped by a laser beam, in electro-optic materials biased by a traveling electromagnetic wave, in acousto-optic materials modulated by an acoustic wave, or in tunable metamaterials controlled by biasing electronic circuits.

The reported unusual electromagnetic modes may find applications in efficient harmonic generators and perfect mixers, as they provide unprecedented control over the generation of electromagnetic harmonics without undesired intermodulation effects. Moreover, since the generated harmonics are exponentially amplified, such modes can be used to produce electromagnetic sources in frequency ranges that are not easily accessible, such as terahertz gaps.

APPENDIX A: COMPUTATION OF DISPERSION CURVES IN AN UNBOUNDED SPACE-TIME-MODULATED LORENTZ MEDIUM

Consider a Lorentz medium with relative permittivity (3), where $\omega_p = e\sqrt{\frac{n_a}{\epsilon_0 m_e}}$ is the plasma frequency, ω_t is the Lorentz resonance frequency, γ is the collision rate, and n_a is the atomic (molecular) density. Assume that n_a is modulated spatiotemporally as in (4), where f_{per} is a periodic function with period 2π . The classical Newton equation describing the polarization density $\mathbf{P}(\mathbf{r}, t)$ in such a medium is described by (7) where \mathbf{E} is the electric field. To find the dispersion relation of the electromagnetic waves propagating in such a medium, (7) is

solved in conjunction with the wave equation in a space-time-varying medium, (5), (6). To find the dispersion relation we use a Floquet-Bloch analysis, expanding all the fields in a series involving infinite space-time harmonics, $e^{j[(\omega+n\omega_m)t-(\beta+n\beta_m)z]}$, as in (8), where $\Psi = \mathbf{E}, \mathbf{P}, \mathbf{D}$, and $\Psi_n = \mathbf{E}_n, \mathbf{P}_n, \mathbf{D}_n$ are unknown complex constants. Next the space-time periodic density (4) is expanded in its Fourier series,

$$n_a(\mathbf{r}, t) = \sum_{n=-\infty}^{\infty} d_n e^{jn(\omega_m t - \beta_m z)}, \quad (\text{A1})$$

where d_n s are the corresponding Fourier coefficients. Then (8) and (A1) are substituted in (7), (5), and (6), and, leveraging the orthogonality of the space-time harmonics, the resulting system of equations is reduced to a matrix equation $\mathbf{A}(\beta, \omega)\mathbf{x} = \mathbf{0}$, where $\mathbf{x} = [\mathbf{E}_n, \dots, \mathbf{P}_n, \dots, \mathbf{D}_n]^T$ is a column vector of the unknown coefficients in (8). To find the dispersion curves at a given frequency ω_i , the nonlinear equation $|\mathbf{A}(\omega_i, \beta)| = 0$ is solved numerically for the unknown β , or equivalently, the dispersion relation for a given β_i can be found by solving the nonlinear equation $|\mathbf{A}(\omega, \beta_i)| = 0$ for the unknown ω . Once solved, the corresponding unknown coefficients $\mathbf{x} = [\mathbf{E}_n, \dots, \mathbf{P}_n, \dots, \mathbf{D}_n]^T$ for the (known) (ω, β) pair are found by solving for the null space of the (singular) matrix $\mathbf{A}(\omega, \beta)$. And finally, the field profiles are determined by substituting $\mathbf{x} = [\mathbf{E}_n, \dots, \mathbf{P}_n, \dots, \mathbf{D}_n]^T$ in (8).

APPENDIX B: ELECTROMAGNETIC FIELD PROFILE OF THE UNUSUAL CODIRECTIONAL-COUPLED ELECTROMAGNETIC MODES

The Floquet-Bloch analysis in Appendix A is used to calculate the dispersion curves and electromagnetic fields for the structures in Figs. 3 and 5 in the main manuscript. The spectrum of the fields for subluminal and superluminal modulations is presented next.

1. Subluminal modulation: Additive and subtractive modes

For the subluminal structure in Fig. 3 in the main manuscript the corresponding field spectrum for the additive and subtractive modes are presented in Fig. 9. Figure 9(a) shows the magnitude spectrum of the additive (solid) and subtractive (dashed) modes. The two harmonics at ω_0 (green), $\omega_0 + \omega_m$ (red) corresponding to the coupled space-time harmonics at the circled intersection in Fig. 2 in the main text ($n = 0$ and $n = -1$) are the strongest, and the rest of the harmonics are more than 50 dB weaker. Figure 9(b) shows the phase difference between the additive and subtractive mode harmonics. The harmonics at ω_0 (green) are in-phase, whereas those at $\omega_0 + \omega_m$ (red) are out of phase. Therefore the field profile of these modes can be effectively represented as (9), (10) in the main manuscript.

2. Superluminal modulation: Growing and decaying modes

For the subluminal structure in Fig. 5 in the main manuscript the corresponding field spectrum for the growing and decaying modes are presented in Fig. 10. Figure 10(a) shows the magnitude spectrum of the growing (solid) and decaying (dashed) modes. The two harmonics at ω_0 (green), $\omega_0 + \omega_m$

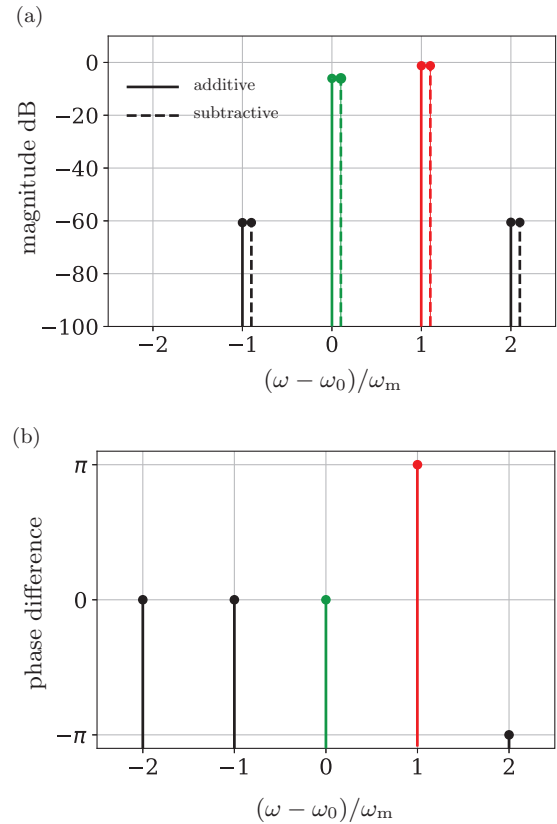


FIG. 9. Magnitude and phase of the harmonics for the additive and subtractive modes in Fig. 2(b). (a) Magnitude of the additive and subtractive modes. For clarity the dashed lines are shifted by 0.1 units. (b) The phase difference between the harmonics of the additive and subtractive modes.

(red) corresponding to the coupled space-time harmonics at the circled intersection in Fig. 4 in the main text ($n = 0$ and $n = -1$) are the strongest, and the rest of the harmonics are more than 50 dB weaker. Figure 10(b) shows the phase difference between the growing and decaying mode harmonics. The harmonics at ω_0 (green) are in-phase, whereas those at $\omega_0 + \omega_m$ (red) are out of phase. Therefore the field profile of these modes can be effectively represented as (11), (12) in the main manuscript.

APPENDIX C: SCATTERING FROM A FINITE SLAB OF A SPACE-TIME-MODULATED LORENTZ MEDIUM: THE MODE-MATCHING ANALYSIS

Consider a slab of space-time-modulated dispersion-engineered Lorentz medium, (3) and (4), sandwiched between two semi-infinite nondispersive media as shown in Fig. 11 and excited by a plane wave $\mathbf{E}^i = \hat{\mathbf{x}}e^{j(\omega t - kz)}$. We represent the electromagnetic fields inside the slab as a superposition of all the modes of the infinite space-time-modulated medium. The wave \mathbf{E}^i incident at the left interface excites the forward-propagating slab modes; these modes are then reflected at the second interface and excite backward-propagating slab modes. Therefore a complete solution of the electromagnetic field inside the slab should contain both forward- and backward-

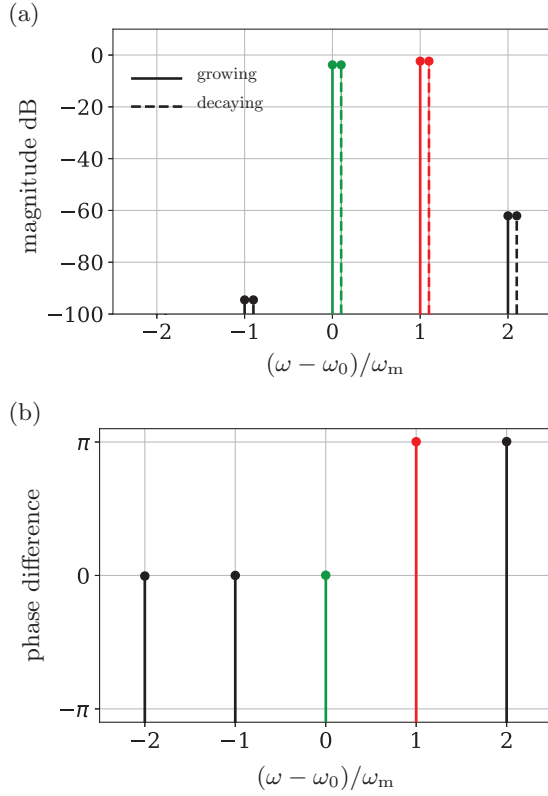


FIG. 10. Magnitude and phase of the harmonics for the growing and decaying modes in Fig. 4(b). (a) Magnitude of the harmonics of the growing and decaying modes. For clarity the dashed lines are shifted by 0.1 units. (b) The phase difference between the harmonics of the growing and decaying modes.

propagating modes. The forward-propagating field inside the slab, $\mathbf{E}^+(z, t)$, is expressed as a superposition of all the forward-propagating modes of the unbounded space-time-modulated medium, $\mathbf{E}_p^+(z, t)$, with unknown coefficients

$$\mathbf{E}^+(z, t) = \sum_{p=-\infty}^{\infty} a_p^+ \mathbf{E}_p^+(z, t). \quad (\text{C1})$$

Similarly, the backward-propagating field inside the slab, $\mathbf{E}^-(z, t)$, is expressed as a superposition of all the backward-propagating modes of the unbounded space-time-modulated

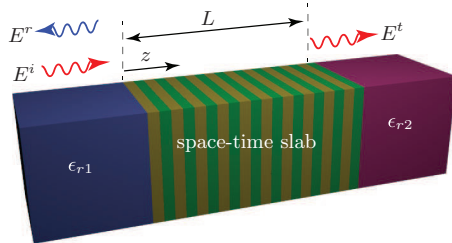


FIG. 11. A slab of space-time-modulated dispersion-engineered medium is sandwiched between two nondispersive media and excited by a forward-propagating wave \mathbf{E}^i . \mathbf{E}^r and \mathbf{E}^t represent reflected and transmitted fields.

medium, $\mathbf{E}_p^-(z, t)$, with unknown coefficients

$$\mathbf{E}^-(z, t) = \sum_{p=-\infty}^{\infty} a_p^- \mathbf{E}_p^-(z, t), \quad (\text{C2})$$

where

$$\mathbf{E}_{p,n}^{\pm}(z, t) = \hat{\mathbf{x}} e^{j(\omega t - \beta_p^{\pm} z)} \sum_{n=-\infty}^{\infty} E_{p,n}^{\pm} e^{jn(\omega_m t - \beta_m z)} \quad (\text{C3})$$

are the forward- (\mathbf{E}_p^+) and backward- (\mathbf{E}_p^-) propagating modes of the infinite space-time-modulated medium, which were calculated in Appendix A.

The reflected and transmitted waves contain all the frequency content of the slab modes, i.e., $\omega_p = \omega_0 + p\omega_m$. Therefore, they are represented as superposition of plane waves at frequencies ω_p with unknown coefficients,

$$\mathbf{E}^r(z, t) = \hat{\mathbf{x}} \sum_{p=-\infty}^{\infty} a_p^r e^{j(\omega_p t + k_p^r z)}, \quad (\text{C4})$$

$$\mathbf{E}^t(z, t) = \hat{\mathbf{x}} \sum_{p=-\infty}^{\infty} a_p^t e^{j(\omega_p t - k_p^t z)}, \quad (\text{C5})$$

where $k_p^r = \omega_p \sqrt{\mu_0 \epsilon_0 \epsilon_{r1}}$ and $k_p^t = \omega_p \sqrt{\mu_0 \epsilon_0 \epsilon_{r2}}$.

Similarly, the magnetic fields inside the slab are represented as a superposition of the forward- and backward-propagating slab modes

$$\mathbf{H}^+(z, t) = \sum_{p=-\infty}^{\infty} a_p^+ \mathbf{H}_p^+(z, t), \quad (\text{C6})$$

$$\mathbf{H}^-(z, t) = \sum_{p=-\infty}^{\infty} a_p^- \mathbf{H}_p^-(z, t), \quad (\text{C7})$$

where the corresponding magnetic fields for each mode [$\mathbf{H}_p^{\pm}(z, t)$] are calculated by applying the Maxwell-Faraday equation to (C3), leading to

$$\mathbf{H}_p^{\pm}(z, t) = \hat{\mathbf{y}} e^{j(\omega t - \beta_p^{\pm} z)} \sum_{n=-\infty}^{\infty} H_{p,n}^{\pm} e^{jn(\omega_m t - \beta_m z)}, \quad (\text{C8})$$

where

$$H_{p,n}^{\pm} = \frac{\beta_p^{\pm} + n\beta_m}{\mu_0(\omega + n\omega_m)} E_{p,n}^{\pm}. \quad (\text{C9})$$

Application of the boundary conditions, i.e., continuity of the tangential electric and magnetic fields at the slab interfaces, then leads to a system of equations for the unknown coefficients, a_p^+ , a_p^- , a_p^r , a_p^t , whose solution provides the reflected and transmitted fields as well as the fields inside the slab.

- [1] J. D. Joannopoulos, S. G. Johnson, J. N. Winn, and R. D. Meade, *Photonic Crystals: Molding the Flow of Light* (Princeton University Press, Princeton, NJ, 2011).
- [2] R. E. Collin, *Foundations for Microwave Engineering* (John Wiley & Sons, New York, 2007).
- [3] R. Kashyap, *Fiber Bragg Gratings* (Academic Press, New York, 2009).
- [4] D. K. Kalluri, *Electromagnetics of Time Varying Complex Media: Frequency and Polarization Transformer* (CRC Press, Boca Raton, FL, 2010).
- [5] J. R. Zurita-Sánchez and P. Halevi, *Phys. Rev. A* **81**, 053834 (2010).
- [6] J. R. Zurita-Sánchez, P. Halevi, and J. C. Cervantes-Gonzalez, *Phys. Rev. A* **79**, 053821 (2009).
- [7] J. Reyes-Ayona and P. Halevi, *Appl. Phys. Lett.* **107**, 074101 (2015).
- [8] E. Cassedy, *Proc. IEEE* **55**, 1154 (1967).
- [9] E. Cassedy and A. Oliner, *Proc. IEEE* **51**, 1342 (1963).
- [10] N. Chamanara, S. Taravati, Z.-L. Deck-Léger, and C. Caloz, *Phys. Rev. B* **96**, 155409 (2017).
- [11] S. Taravati, N. Chamanara, and C. Caloz, *Phys. Rev. B* **96**, 165144 (2017).
- [12] C. Caloz, *Proc. IEEE* **99**, 1711 (2011).
- [13] C. Caloz, S. Gupta, Q. Zhang, and B. Nikfal, *IEEE Microw. Mag.* **14**, 87 (2013).
- [14] A. Säynätjoki, M. Mulo, J. Ahopelto, and H. Lipsanen, *Opt. Express* **15**, 8323 (2007).
- [15] M. Ebnali-Heidari, C. Grillet, C. Monat, and B. Eggleton, *Opt. Express* **17**, 1628 (2009).
- [16] C. Caer, X. Le Roux, D. Marris-Morini, N. Izard, L. Vivien, D. Gao, E. Cassan *et al.*, *IEEE Photon. Technol. Lett.* **23**, 1298 (2011).
- [17] J. D. Jackson, *Classical Electrodynamics* (John Wiley & Sons, New York, 2007).
- [18] C. Caloz and T. Itoh, *Electromagnetic Metamaterials: Transmission Line Theory and Microwave Applications* (John Wiley & Sons, New York, 2005).
- [19] D.-W. Wang, H.-T. Zhou, M.-J. Guo, J.-X. Zhang, J. Evers, and S.-Y. Zhu, *Phys. Rev. Lett.* **110**, 093901 (2013).
- [20] B. E. Saleh and M. C. Teich, *Fundamentals of Photonics*, Vol. 22 (Wiley, New York, 1991).
- [21] G. Trainiti and M. Ruzzene, *New J. Phys.* **18**, 083047 (2016).
- [22] J. N. Winn, S. Fan, J. D. Joannopoulos, and E. P. Ippen, *Phys. Rev. B* **59**, 1551 (1999).
- [23] Z. Yu and S. Fan, *Nat. Photon.* **3**, 91 (2009).